High-resolution magnetic resonance histology of the embryonic and neonatal mouse: A 4D atlas and morphologic database

Alexandra E. Petiet*†, Matthew H. Kaufman‡, Matthew M. Goddeeris§, Jeffrey Brandenburg*, Susan A. Elmore¶, and G. Allan Johnson*†‖**

*Center for *In Vivo* Microscopy and Departments of §Cell Biology and ‖Radiology, Duke University Medical Center, Box 3302, Durham, NC 27710; †Department of Biomedical Engineering, Duke University, Box 90281, Durham, NC 27708; ‡Department of Biomedical Sciences, University of Edinburgh, Hugh Robson Building, George Square, Edinburgh EH8 9XD, United Kingdom; and ¶Laboratory of Experimental Pathology, National Institute of Envrionmental Health Sciences, Box 12233, Maildrop B3-06, 111 T.W. Alexander Drive, Research Triangle Park, NC 27709

Communicated by William Happer, Princeton University, Princeton, NJ, June 16, 2008 (received for review December 10, 2007)

Engineered mice play an ever-increasing role in defining connections between genotype and phenotypic expression. The potential of magnetic resonance microscopy (MRM) for morphologic phenotyping in the mouse has previously been demonstrated; however, applications have been limited by long scan times, availability of the technology, and a foundation of normative data. This article describes an integrated environment for high-resolution study of normal, transgenic, and mutant mouse models at embryonic and neonatal stages. Three-dimensional images are shown at an isotropic resolution of 19.5 μm (voxel volumes of 8 pL), acquired in 3 h at embryonic days 10.5–19.5 (10 stages) and postnatal days 0–32 (6 stages). A web-accessible atlas encompassing this data was developed, and for critical stages of embryonic development (prenatal days 14.5–18.5), >200 anatomical structures have been identified and labeled. Also, matching optical histology and analysis tools are provided to compare multiple specimens at multiple developmental stages. The utility of the approach is demonstrated in characterizing cardiac septal defects in conditional mutant embryos lacking the *Smoothened* receptor gene. Finally, a collaborative paradigm is presented that allows sharing of data across the scientific community. This work makes magnetic resonance microscopy of the mouse embryo and neonate broadly available with carefully annotated normative data and an extensive environment for collaborations.

digital atlas | magnetic resonance microscopy | mouse embryo

In their seminal papers on MRI, Lauterbur (1) and Mansfield and Grannell (2) recognized the potential for magnetic resonance microscopy (MRM). Almost 13 years later, theory was reduced to practice with acquisition of the first MRI scans at microscopic spatial resolution (3–5). Some of the first applications of MRM focused on the developing mouse embryo (6, 7). The advent of 3D imaging methods spurred additional interest as its utility in understanding complex anatomy became apparent (8). Since these early studies, using MRM to understand the developing embryo has grown steadily. MRM has been used for 3D studies in embryos at embryonic (E) day 10.5 and later when confocal techniques are not viable. Unfortunately, routine use of MRM for morphologic phenotyping has been limited to locations with expensive equipment and infrastructure.

Spatial resolution, acquisition time, and field of view (FOV) are three closely related barriers that have limited the utility of MRM. Several laboratories have explored using MRM to image the mouse embryo with widely varying resolution and acquisition time (9–14). The trade-off between spatial resolution and acquisition time is complicated by many factors (15). For a constant signal-to-noise ratio, doubling the resolution along all three axes increases acquisition time 64-fold. As a consequence, the majority of studies have been at relatively low resolution (>40-μm isotropic voxels at 64 pL). Resolution as high as 25 μm (voxel volume of 16 pL) has been reported in the E15.5 embryo (16–18) but required 9 h to acquire data. Johnson *et al.* (19) achieved a general solution to this problem by introducing an active staining method to enhance the signal, and Petiet *et al.* (20) extended the technique to the rat fetus to obtain 3D image arrays at 19.5-μm isotropic resolution (7.4 pL) in 3 h.

The spatial resolution depends on the FOV. The earliest 3D images were acquired over a $5 \times 5 \times 5$-mm^3 FOV using $256 \times 256 \times 256$ image arrays (9). A spatial resolution of 20 μm was achieved with this limited FOV. Although sufficient for an E9.5 embryo, this resolution could not be readily extended to larger specimens. For example, imaging an E18.5 embryo at the same spatial resolution would require image arrays of $1{,}024 \times 512 \times 512$ for a FOV of $20 \times 10 \times 10$ mm^3. In turn, this presents logistical problems in acquisition, reconstruction, archival, display, and analysis. The raw data file for a fully sampled $1{,}024 \times 512 \times 512$ array is >4 GB, with a reconstructed image >500 MB. Acquisition and reconstruction software for such large arrays is not commercially available, and hardware and software for comparative analysis are not yet widely deployed.

An additional barrier to widespread use of MRM in phenotyping the mouse embryo is availability of a standardized knowledge base. The introduction of computed tomography in 1973 caused physicians to rethink their view of anatomy as plain film images were replaced with transverse sections. Magnetic resonance imaging required an additional knowledge base for interpretation of anatomy in alternative coronal and sagittal planes with widely varied image contrast. The database presented has been designed to accelerate this process for interpreting mouse embryo images.

We present here methods that we believe will significantly enhance the use of MRM to study the mouse embryo, including the following:

1. A standardized protocol based on actively stained specimens that allows acquisition of images at a resolution of 19.5 μm in ~3 h.
2. A 4D atlas at E10.5 to postnatal day (PND) 32 (total of 16 stages). Image sets at E10.5–E18.5 are annotated with >200 labels.
3. An Internet portal for the atlas that is analogous to the gene sequence databases, which addresses challenges unique to digital imaging.

Author contributions: G.A.J. designed research; A.E.P. performed research; M.M.G. and J.B. contributed new reagents/analytical tools; M.H.K., M.M.G., and S.A.E. analyzed data; and A.E.P. and G.A.J. wrote the paper.

The authors declare no conflict of interest.

**To whom correspondence should be addressed. E-mail: gaj@orion.duhs.duke.edu.

This article contains supporting information online at www.pnas.org/cgi/content/full/0805747105/DCSupplemental.

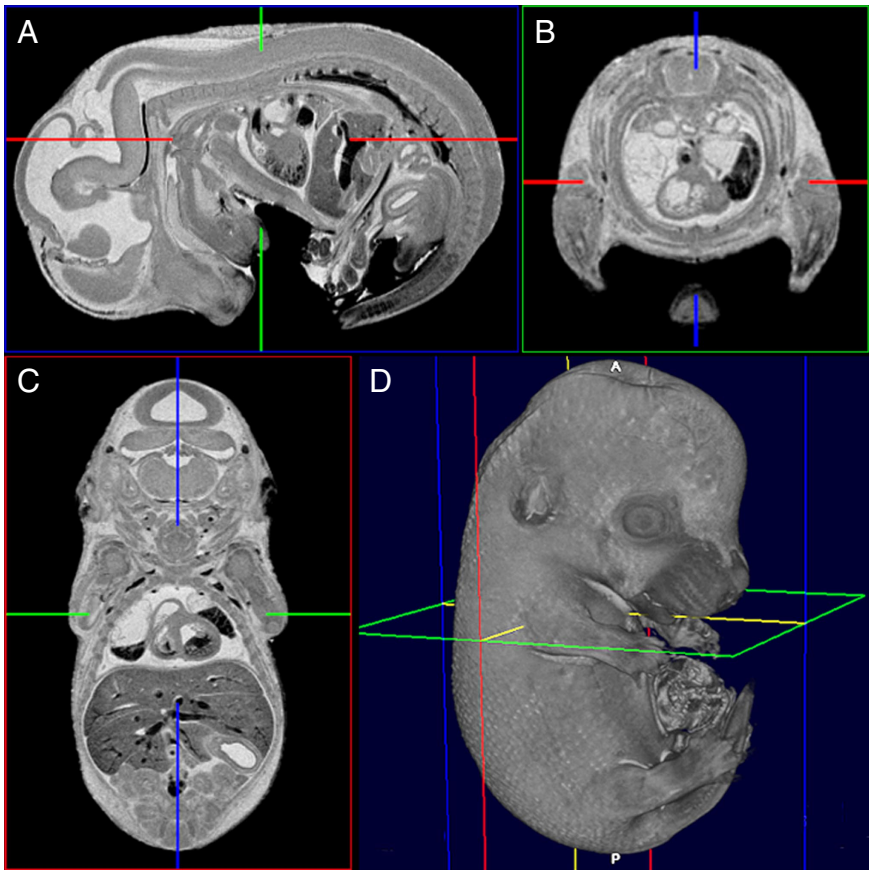

Fig. 1. Magnetic resonance imaging scans of an E15.5 mouse at 19.5-μm resolution. A 3D isotropic dataset was acquired in 3 h, 11 min with a matrix size of 1,024 $\times$ 512 $\times$ 512 and FOV of 20 $\times$ 10 $\times$ 10 mm^3. Views displayed include the following: sagittal (*A*), transverse (*B*), coronal (*C*), and volume rendered (*D*).

Results

Fig. 1 *A–C* shows sagittal, transverse, and coronal images of a stained E15.5 mouse. The high-throughput protocol was used for scans with an isotropic resolution of 19.5 μm. Because the resolution is equivalent in all three cardinal planes, one can retrospectively define the plane along any arbitrary axis. Fig. 1*D* shows a volume image demonstrating the intersection of the three planes. The signal-to-noise ratio of 50:1 and the contrast-to-noise ratio are sufficient to identify all major organs.

Fig. 2 presents representative midsagittal images of embryonic

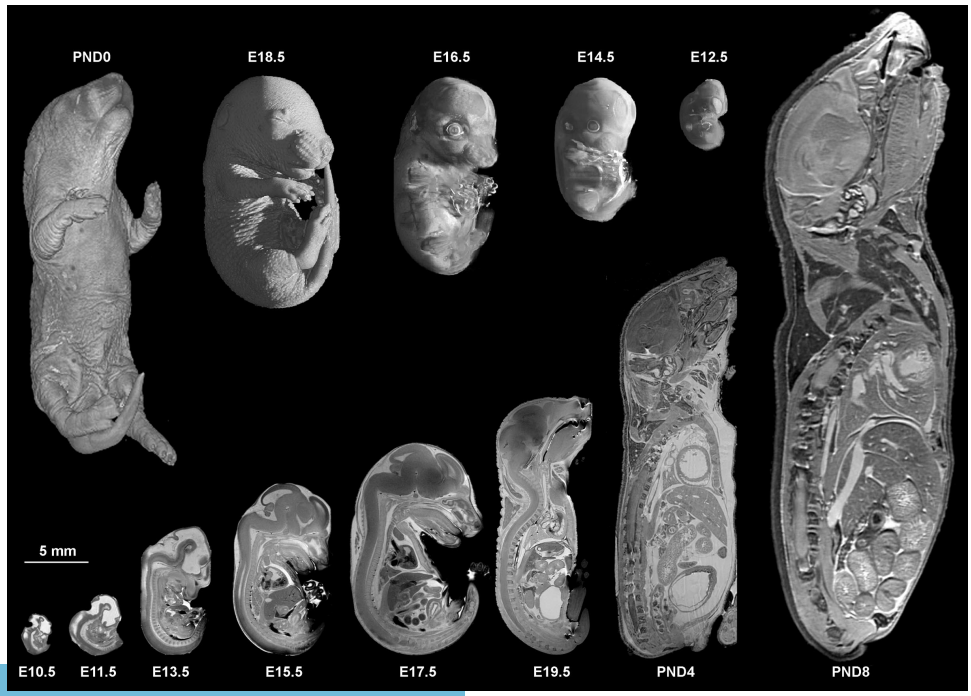

Fig. 2. Midsagittal slices from volume datasets and surface views of the developing mouse at selected stages (E10.5–PND8).

specimens acquired with the archival protocol with two excitations (see *Materials and Methods*) and postnatal specimens acquired with the standard protocol. This abbreviated selection illustrates the challenge of scale encountered when imaging at E10.5, where the average crown-to-rump length is 4 mm vs. PND8 with a crown-to-tail dimension of 40 mm and the PND32 mouse (data not shown) with a 75-mm crown-to-tail length [supporting information (SI) Table S1].

The volumes have been assembled into a 4D atlas (3D volume in space plus time postconception as the fourth dimension). More than 200 structures have been labeled by using accepted nomenclature (21) for stages E14.5–E18.5. Labels are supplied for all three cardinal planes at intervals ranging from 195 to 585 μm. The software that displays the annotated data was adapted from the Mouse Biomedical Informatics Research Network (MBIRN) Atlasing Toolkit (MBAT) (http://www.nbirn.net/tools/mbat/index.shtm). Fig. 3 shows the display tool with a representative slice from the labeled E16.5 specimen.

Fig. 4 demonstrates use of the atlas to study developmental changes in the heart. Coronal and transverse views from E12.5, E18.5, PND0, and PND4 specimens are displayed simultaneously, allowing interactive matching of anatomical landmarks. Larger structures, such as the atria and ventricles visible in postnatal specimens (Fig. 4 *E–H*), assist in localizing these features at earlier developmental time points (Fig. 4 *A–D*). As smaller structures develop, like the aortic valve (Fig. 4 *E* and *F*) and tricuspid and mitral valves (Fig. 4 *G* and *H*), the isotropic resolution and multiple-plane views facilitate confident identification of the landmarks.

The value of the 4D atlas in probing the complex interplay between genotype and morphologic phenotype is shown in a study of cardiac malformations. Images of embryonic cardiac septal defects were acquired by using a mouse strain bearing a conditional ablation of the *Smo* receptor gene. Fig. 5 shows images from E14.5 WT and *Smo*$^{-}$ specimens acquired with the standard 3-h protocol. Severe septal defects are identified in the mutant in three regions. In most cranial slices (Fig. 5 *A* and *B*), the outflow tract, which branches into the aorta and pulmonary trunk in the WT, appears as a single outflow tract in the mutant. In views of the center of the heart (Fig. 5 *C* and *D*), the mutant shows an open interventricular septum. In most caudal slices (Fig. 5 *E* and *F*), the dorsal mesenchymal protrusion (an undercharacterized structure overlying the endocardial cushions) (22) is absent in the *Smo*$^{-}$ specimen. The rendered volumes of segmented structures (Fig. 5 *A′*, *B′*, *E′*, and *F′*) provide added views of the morphologic consequences of the mutation.

Fig. 6 is a collage from the web-based tools assembled by using the 4D atlas. The core of the software is VoxPort, a Structured Query Language (SQL) database developed by MRPath Inc. (now Umlaut Inc.). Access to the database is provided for free at http://www.civm.duhs.duke.edu/devatlas/index.html. Registered users can download MBAT software to access the entire 4D mouse atlas. VoxStation, a Java application, allows simultaneous display of images from multiple stages obtained with various imaging modalities. Users can segment regions of interest, reconstruct structures in 3D with third-party software [e.g., ImageJ (http://rsb.info.nih.gov/ij)], and make quantitative assessments of morphology changes. Other investigators can add datasets with novel phenotypes. As imaging technology advances and knowledge of gene-based morphology in the mouse expands, the infrastructure to incorporate this new information is now in place.

Discussion

Many investigators have demonstrated MRI scans of the mouse embryo. The scan times in these previous studies have been too long for routine use (9–36 h). Spatial resolution has been limited (25–120 μm), and the contrast has varied (rapid acquisition relaxation-enhanced, T2-weighted, diffusion-weighted, and proton density). These previous studies used relatively small image matrices that either limited the FOV, spatial resolution, or both. Combining active staining with extended dynamic range partial Fourier acquisition has allowed us to acquire the highest resolution images yet obtained, with the largest image matrices covering the largest FOV, with an acquisition time far shorter than previous studies. Our preparation for prenatal specimens is

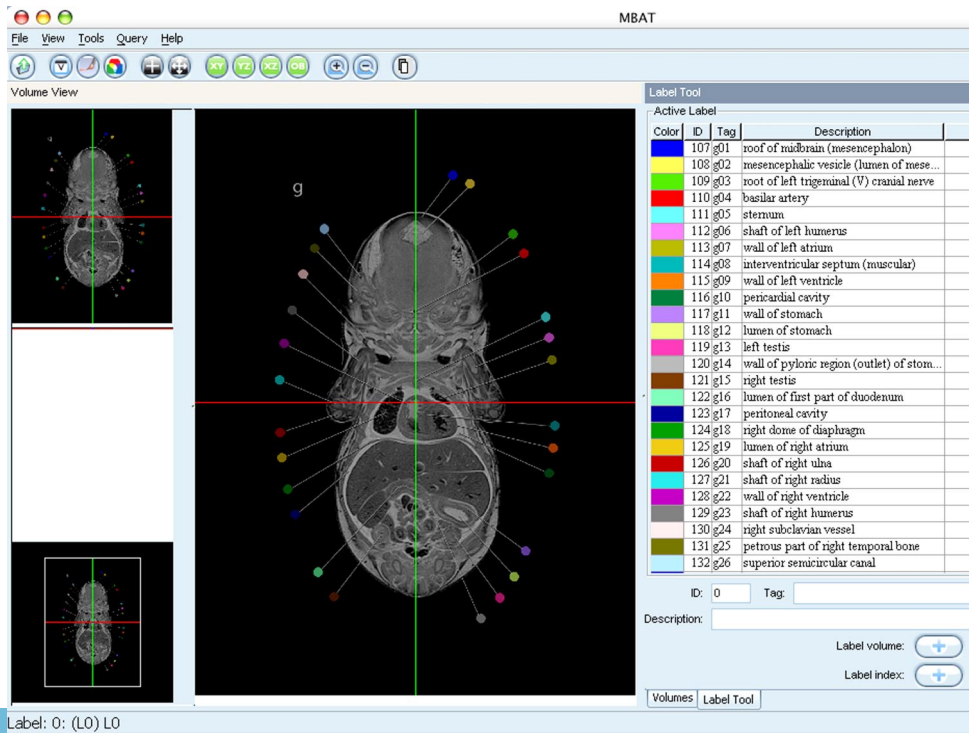

Fig. 3. Representative image from the labeled 4D atlas of the mouse shows a coronal slice from an E16.5 specimen.

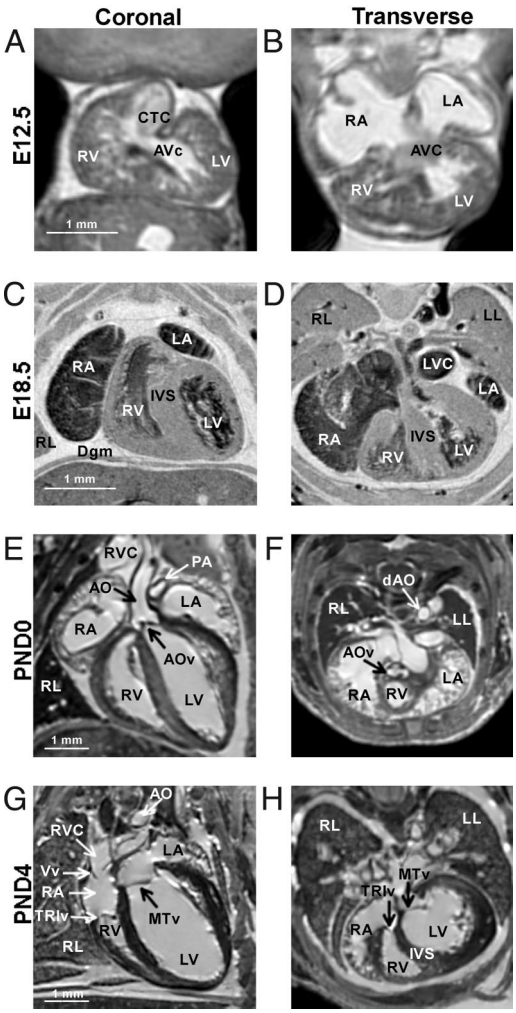

Fig. 4. Magnetic resonance imaging scans of normal mice (E12.5, E18.5, PND0, PND4) displayed as coronal (*Left*) and transverse (*Right*) slices through the heart. Anatomical structures in *A* and *B* include the following: AVc, atrioventricular canal; CTC, conotruncus cushions; LV, (primitive) left ventricle (trabeculated wall of common ventricular chamber); RV, (primitive) right ventricle (trabeculated wall of bulbus cordis); RA, right atrium; LA, left atrium; AVC, atrioventricular cushions. Anatomical structures in *C* and *D* include the following: IVS, interventricular septum; Dgm, dome of diaphragm; LVC, left superior vena cava; LL, lobe of left lung; RL, lobe of right lung. Anatomical structures in *E* and *F* include the following: AO, aorta; AOv, aortic valve; PA, pulmonary artery; RVC, right superior vena cava; dAO, descending aorta. Anatomical structures in *G* and *H* include the following: MTv, mitral valve; TRIv, tricuspid valve; Vv, leaflets of venous valve.

fast (<1 h) and easy to perform. Although transcardial perfusion for postnatal mice requires more technical skill, it is still a rapid procedure of approximately 1 h per animal. Both procedures are readily scalable to large numbers of specimens.

The work expands on work by others. Dhenain *et al.* (13) published an MRI atlas of the mouse embryo (E6–E15.5). The atlas shown here has eight times higher spatial resolution, covering not only early embryonic and fetal stages but following through the critical first 32 days of postnatal development. Other investigators have provided annotation to help interpret the MRI signals and complex anatomy (13, 14, 23). The atlas described here is the most comprehensive to date, identifying >200 structures at five different stages in three planes, along with complementary conventional histology.

There is little doubt that the mouse will serve as a critical link between genotype and phenotype. However, as seen in the evolution of clinical imaging methods, wide variation in protocols can slow the broad use of a new method. Several groups have demonstrated the utility of MRM to study cardiac malformations in the mouse (17, 18, 24). We used a model with cardiac septal defects to demonstrate the value of our standard protocol in a high-throughput environment. We do not claim that the protocol is the optimal solution. However, the protocol does have several appealing attributes—substantially higher spatial resolution than work published to date, and it can be executed in ~3 h. Even higher throughput will be readily achieved in the near term. Schneider *et al.* (25) have demonstrated the simultaneous acquisition of 32 specimens by using a single radiofrequency coil. Bock *et al.* (26) demonstrated an even superior method using multiple individual coils. At this point, the limit is the homogeneous volume of the magnetic field and the linear volume of the gradient coils. Our magnet and gradients can readily accommodate two to four embryos. With an automated sample changer, we could acquire up to 32 images per day. At that point, the bottleneck for screening will arise in interpretation. The final benefit of this protocol is uniform high contrast. The staining process clearly differentiates >200 structures, which are visible throughout development. Because the stain reduces the T1 of all the tissues, the contrast predominantly depends on proton density and diffusion. Thus, the protocol will provide similar results regardless of the field strength at which the images are acquired.

In 1991, we introduced the concept of spin echo imaging with "very large arrays," which is pale compared with our needs today. To simultaneously decrease the voxel size by >10-fold over our previous work while increasing the FOV to allow coverage of a PND32 mouse, we have increased the image array by 64-fold. The infrastructure required was appropriately scaled. New acquisition software was developed to accommodate the much broader dynamic range required. The reconstruction software has been appropriately scaled. A sophisticated imaging database has been constructed with >1.3 TB now online. These resources are of no value unless the scientific community can have ready access, however. By placing the burden of volume and image management on our local image server, users with limited computational power and memory can still interactively page, in space and time, through multigigabyte image arrays.

Finally, we have introduced an approach to a collaborative community of science. As a National Biomedical Technology Resource, the Center for *In Vivo* Microscopy is committed to making our tools and expertise as widely available as possible. Investigators can contact us via the web to collaborate on scanning new embryos. The specimens, once scanned, are available to these collaborators and the rest of the scientific community through the infrastructure described here. The atlas with labels provides expert guidance in identifying normal anatomy. Perhaps most significantly, the same infrastructure allows our collaborators to contribute back to the archive. As data are analyzed, investigators can label and comment on their own data. Additional supplemental data, such as volume measures, conventional histology, volume visualization, and animations, can all be added. We expect that users will, as we have in this article, make their data available to their colleagues upon publication. In this traditional article, we have been able to present only a few cross-sections of our acquired data. Our portal lets investigators browse and download our entire multimodality, multiple time point, multigigabyte collection of data and contribute their own observations and analysis back to it. This is a dynamic web resource in which many will contribute to expand our understanding of the developing mouse embryo.

Materials and Methods

Specimen Preparation. All procedures were approved by the Duke Institutional Animal Care and Use Committee. Pregnant C57BL/6 dams were obtained from

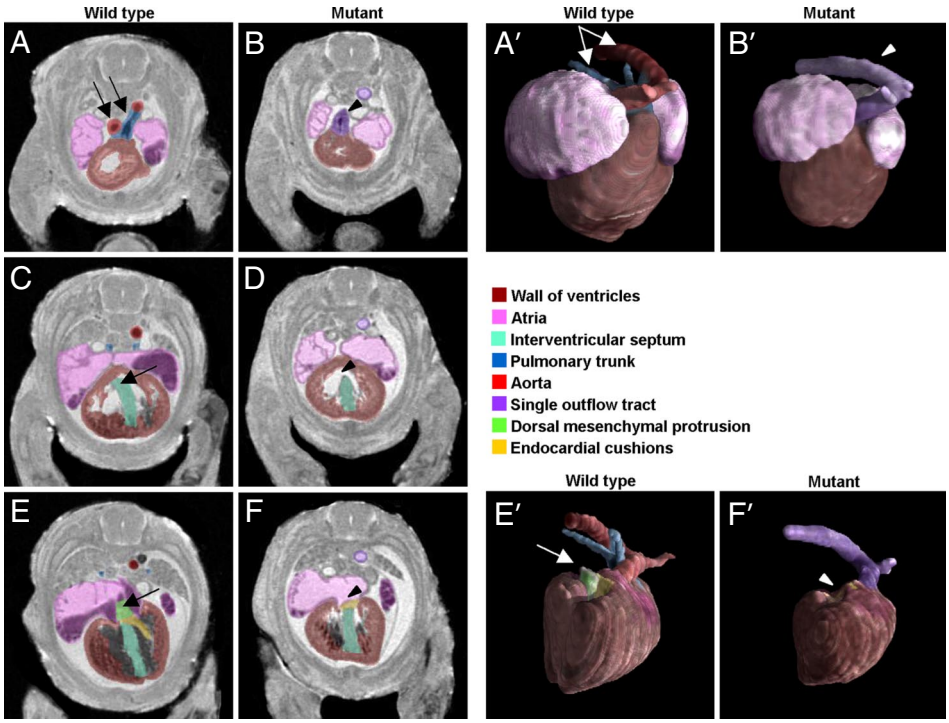

Fig. 5. Magnetic resonance imaging scans of WT and *Smo*$^{-}$ mutant mouse embryos at E14.5. Arrows point out normal structures in WT specimens (*A*, *A′*, *C*, *E*, and *E′*); arrowheads, which point to corresponding anatomy in images of the mutant strain (*B*, *B′*, *D*, *F*, and *F′*), direct attention to cardiac septal defects. Images *A*–*F* are transverse slices through the region of the heart, progressing from most cranial (*A* and *B*) to most caudal (*E* and *F*). *A′*–*F′* are volume-rendered illustrations of the segmented hearts, ventral (*A′* and *B′*) and dorsal (*E′* and *F′*) views. These images were rotated by 90° relative to transverse images, with the long axis of the heart now vertical (apex down). Dorsal views are presented with the atria removed for clearer visualization of the dorsal mesenchymal protrusion.

Charles River Laboratories. Embryos from days 10.5–19.5 (10 prenatal stages total, at 1-day increments) were extracted after laparotomy. Embryos were dissected in ice-cold saline and then immersion fixed in a mixture of fixative (Bouin's solution; LabChem) and a paramagnetic contrast agent (ProHance, gadoteridol; Bracco Diagnostics) (20). E19.5 fetuses were killed with i.p. pentobarbital at 500 mg/kg and perfused by i.p. and s.c. injections of the fixing and staining mixture, followed by overnight immersion in the same solution.

Mouse neonates PND0, 2, 4, 8, 16, and 32 (six postnatal stages total) were

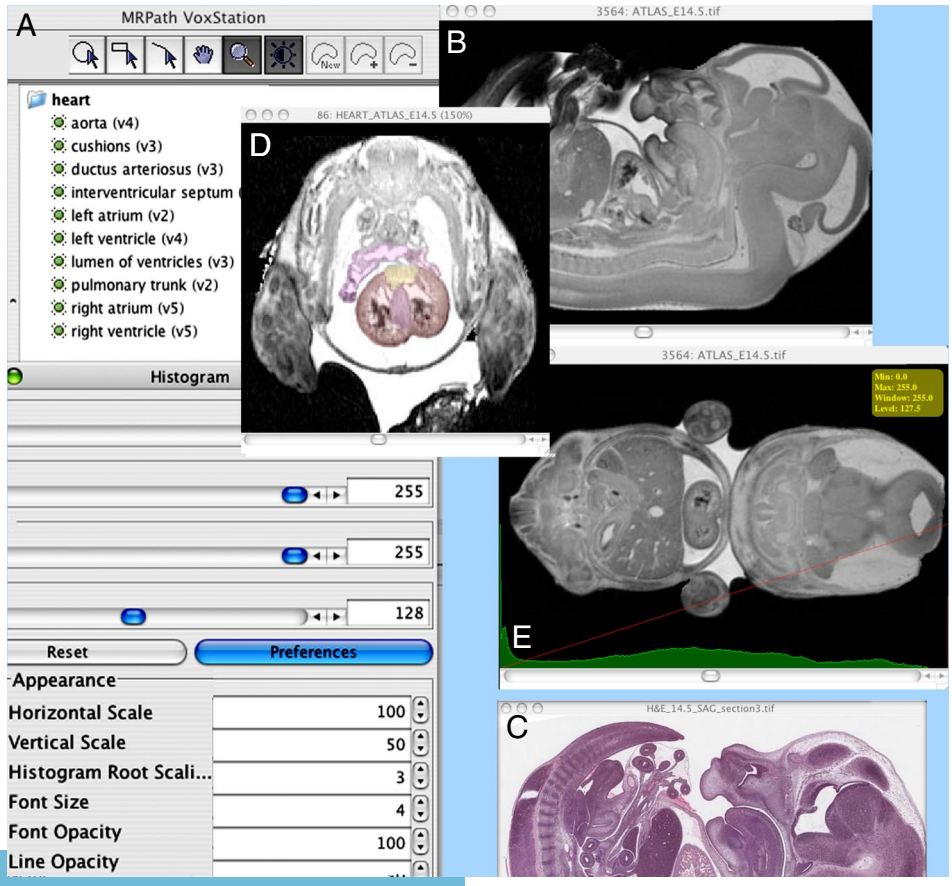

Fig. 6. Selected illustrations of mouse atlas image manipulation using VoxPort and VoxStation. (*A* and *D*) Drawing and annotation tools allow labeling and annotation. (*A* and *E*) Contrast can be optimized by interactive manipulation of the window and level of the histogram. (*B* and *C*) A sagittal slice from an MRI view of an E14.5 specimen (*B*) compared with an H&E section (*C*).

perfusion fixed and stained using ultrasound-guided transcardiac perfusion, according to the methods described by Zhou *et al.* (27) using an ultrasound biomicroscope (Vevo 770; VisualSonics). Isoflurane was administered by nose cone. Three different perfusates were delivered through a syringe pump. The left ventricle was perfused for 5 min with a mixture of saline with 0.1% heparin and ProHance to allow infusion with intact circulation. This step used a high concentration of contrast agent (10:1 vol/vol saline/ProHance) and low flow rate. This was followed by perfusion with a 20:1 saline/ProHance mixture at a higher flow rate with outflow from the left jugular vein and the two femoral veins, replacing blood with the perfusate, with a dye included to monitor flush-out. Once this perfusate ran clear, animals were fixed for 10–15 min with formalin and ProHance (20:1 vol/vol concentration). Flow rates were empirically determined and varied as a function of the pup's age (Table S1).

Mutant Embryos. Mutant embryos with conditional ablation of the *Smo* receptor gene were obtained by crossing *Mef2C-AHF-Cre;Smo*$^{-/+}$ male mice with *Smo*$^{flox/flox}$*; R26R/R26R* female Institute of Cancer Research (ICR)-outbred mice (28–30). Three WT and three mutant (*Mef2C-AHF-Cre;Smo*$^{flox/-}$) littermates were collected at E14.5 and prepared by immersion, as described. Tail snips were used for genotyping (30).

MRI. Three-dimensional data for all specimens up to PND8 were acquired at 9.4 T (400 MHz), using a GE EXCITE console (Epic 11.0). PND16 and PND32 were scanned in a 7-T (300 MHz) system, GE EXCITE console (Epic 12.4), with gradients that accommodate larger animals. We used a 3D rf refocused sequence, with asymmetrical sampling and an expanded dynamic range (20) (repetition time = 75 ms, echo time = 5.2 ms), which provides full resolution at the Nyquist frequency. For all embryonic stages, the matrix size was 1,024 × 512 × 512 and FOV was 20 × 10 × 10 mm^3, which yielded an isotropic resolution of 19.5 μm. For routine scans, we used one excitation per view with a scan time of 3 h 11 min. Archival scans of embryonic specimens included in this database were obtained by using two excitations (scan time of 6 h 22 min). Matrix sizes were increased and spatial resolution was decreased to accommodate postnatal animals. Scan time was 3 h 11 min for PND0–8 and increased to 12 h, 24 min for the largest specimens (PND16 and PND32), which required the largest image arrays. Isotropic resolution for postnatal specimens was 39 μm for PND0–4 and 48.8 μm for PND8–32 (Table S1).

Image Processing and Analysis. Datasets were aligned so that the center of the object coincided with the center of the matrix. Arrays were rotated so that the crown-rump axis was aligned with the vertical axis of the array. Selected slices were labeled in three orthogonal planes according to Kaufman's atlas of the developing mouse (21).

Embryonic and neonatal heart volumes were manually labeled by using VoxPort software. Masks were used to segment the labeled hearts from the whole volumes via MATLAB (MathWorks). Volume-rendered images and 3D movies were generated by using VGStudio MAX (Volume Graphics).

ACKNOWLEDGMENTS. We thank Dr. Erik Meyers (Cell Biology and Pediatrics, Duke University) for providing the *Mef2C-AHF-Cre;Smo*$^{+/-}$ mutant embryos; Maggie Lin (Biomedical Engineering, Duke University) for tracing hearts on VoxStation; Dr. Laurence Hedlund and Boma Fubara for help in preparing specimens; Gary Cofer and Sally Gewalt for acquisition assistance, and Sally Zimney for editing assistance. This work was supported by National Institutes of Health/National Center for Research Resources Grant P41 RR005959, National Cancer Institute Grant U24 CA092656, Mouse Biomedical Informatics Research Network Grant U24 RR021760, the Intramural Research Program of the National Institutes of Health/National Institute of Environmental Health Sciences, and National Institutes of Health/National Institute of Child Health and Development Grant R01 HD042803 (to M.M.G.).

1. Lauterbur PC (1973) Image formation by induced local interactions—examples employing nuclear magnetic resonance. *Nature* 242:190–191.
2. Mansfield P, Grannell PK (1975) Diffraction in microscopy in solids and liquids by NMR. *Phys Rev B* 12:3618–3634.
3. Aguayo JB, Blackband SJ, Schoeniger J, Mattingly MA, Hintermann M (1986) Nuclear magnetic resonance imaging of a single cell. *Nature* 322:190–191.
4. Johnson GA, Thompson MB, Gewalt SL, Hayes CE (1986) Nuclear magnetic resonance imaging at microscopic resolution. *J Magn Reson* 68:129–137.
5. Eccles CD, Callaghan PT (1986) High resolution imaging: the NMR microscope. *J Magn Reson* 68:393–398.
6. Johnson GA, Bone SN, Thompson MB (1986). *Magnetic Resonance of the Reproductive System*, eds McCarthy S, Haseltine F (Slack, Inc., Thorofare, NJ), pp 137–141.
7. Effmann EL, Johnson GA, Smith BR, Talbot GA, Cofer GP (1988) Magnetic resonance microscopy of chick embryos in ovo. *Teratology* 38:59–65.
8. Suddarth SA, Johnson GA (1991) Three-dimensional MR microscopy with large arrays. *Magn Reson Med* 18:132–141.
9. Smith BR, Johnson GA, Groman EV, Linney EA (1994) Magnetic resonance microscopy of mouse embryos. *Proc Natl Acad Sci USA* 91:3530–3533.
10. Smith B, Linney E, Huff D, Johnson G (1996) Magnetic resonance microscopy of embryos. *Comput Med Imaging Graph* 20:483–490.
11. Orita J, Sato E, Saburi S, Nishida T, Toyado Y (1996) Magnetic resonance imaging of the internal structures of the mouse fetus. *Exp Anim* 45:171–174.
12. Jacobs RE, Ahrens ET, Dickinson ME, Laidlaw D (1999) Towards a microMRI atlas of mouse development. *Comput Med Imaging Graph* 23:15–24.
13. Dhenain M, Ruffins SW, Jacobs RE (2001) Three-dimensional digital mouse atlas using high-resolution MRI. *Dev Biol* 232:458–470.
14. Schneider JE, *et al.* (2003) High-resolution, high-throughput magnetic paragraph sign resonance imaging of mouse embryonic paragraph sign anatomy using a fast gradient-echo sequence. *MAGMA* 16:43–51.
15. Callaghan PT (1991) *Principles of Nuclear Magnetic Resonance Microscopy* (Oxford Univ Press, New York).
16. Schneider JE, *et al.* (2003) Rapid identification and 3D reconstruction of complex cardiac malformations in transgenic mouse embryos using fast gradient echo sequence magnetic resonance imaging. *J Mol Cell Cardiol* 35:217–222.
17. Schneider JE, *et al.* (2003) High-resolution imaging of normal anatomy, and neural and adrenal malformations in mouse embryos using magnetic resonance microscopy. *J Anat* 202:239–247.
18. Schneider JE, Bhattacharya S (2004) Making the mouse embryo transparent: Identifying developmental malformations using magnetic resonance imaging. *Birth Defects Res C Embryo Today* 72:241–249.
19. Johnson GA, Cofer GP, Gewalt SL, Hedlund LW (2002) Morphologic phenotyping with magnetic resonance microscopy: The visible mouse. *Radiology* 222:789–793.
20. Petiet A, Hedlund LW, Johnson GA (2007) Staining methods for magnetic resonance microscopy of the rat fetus. *J Magn Reson Imaging* 25:1192–1198.
21. Kaufman MH (1992) *The Atlas of Mouse Development* (Academic, London).
22. Wessels A, *et al.* (2000) Atrial development in the human heart: An immunohistochemical study with emphasis on the role of mesenchymal tissues. *Anat Rec* 259:288–300.
23. Zhang J, *et al.* (2003) Three-dimensional anatomical characterization of the developing mouse brain by diffusion tensor microimaging. *NeuroImage* 20:1639–1648.
24. Huang GY, *et al.* (1998) Alteration in connexin 43 gap junction gene dosage impairs conotruncal heart development. *Dev Biol* 198:32–44.
25. Schneider JE, *et al.* (2004) Identification of cardiac malformations in mice lacking Ptdsr using a novel high-throughput magnetic resonance imaging technique. *BMC Dev Biol* 4:16–25.
26. Bock NA, Konyer NB, Henkelman RM (2003) Multiple-mouse MRI. *Magn Reson Med* 49(1):158–167.
27. Zhou YQ, *et al.* (2004) Ultrasound-guided left-ventricular catheterization: A novel method of whole mouse perfusion for microimaging. *Lab Invest* 84:385–389.
28. Zhang XM, Ramalho-Santos M, McMahon AP (2001) Smoothened mutants reveal redundant roles for Shh and Ihh signaling including regulation of L/R symmetry by the mouse node. *Cell* 106:781–792.
29. Verzi MP, McCulley DJ, De Val S, Dodou E, Black BL (2005) The right ventricle, outflow tract, and ventricular septum comprise a restricted expression domain within the secondary/anterior heart field. *Dev Biol* 287:134–145.
30. Goddeeris MM, Schwartz R, Klingensmith J, Meyers EN (2007) Independent requirements for Hedgehog signaling by both the anterior heart field and neural crest cells for outflow tract development. *Development* 134:1593–1604.